

Thermoelectric properties of $\text{Sr}_{n+1}\text{Ti}_n\text{O}_{3n+1}$ ($n=1, 2, 3, \infty$) Ruddlesden–Popper Homologous Series



A.H. Reshak ^{a, b, *}

^a New Technologies – Research Centre, University of West Bohemia, Univerzitni 8, 306 14 Pilsen, Czech Republic

^b Center of Excellence Geopolymer and Green Technology, School of Material Engineering, University Malaysia Perlis, 01007 Kangar, Perlis, Malaysia

ARTICLE INFO

Article history:

Received 12 June 2014

Accepted 3 November 2014

Available online

Keywords:

$\text{Sr}_{n+1}\text{Ti}_n\text{O}_{3n+1}$ ($n=1, 2, 3, \infty$) Ruddlesden–Popper Homologous
Transport properties
Seebeck coefficient

ABSTRACT

The transport properties of $\text{Sr}_{n+1}\text{Ti}_n\text{O}_{3n+1}$ ($n=1, 2, 3, \infty$) Ruddlesden–Popper Homologous Series were evaluated using the semi-classical Boltzmann theory as implemented in the BoltzTraP code. Based on the electronic band structure calculations, we have calculated the charge carrier's concentration at 300, 600 and 900 K, and found that the $\text{Sr}_4\text{Ti}_3\text{O}_{10}$ compound exhibit the highest charge carrier's concentration along the temperature scale.

We also have calculated the electrical conductivity and electronic thermal conductivity at 300, 600 and 900 K, and found that in the vicinity of Fermi level these materials exhibit the minimum value of electrical conductivity and electronic thermal conductivity, which is represent the regions where the investigated materials can give its maximum efficiency. For all compounds the highest value of Seebeck coefficient occurs at 300 K then it decreases with increasing the temperature. We have calculated the power factor (P) at 300, 600 and 900 K, and found that beyond the vicinity of Fermi level these materials exhibit the maximum value of P , which is represent the regions where the investigated materials can give its maximum efficiency. We notice that Sr_2TiO_4 compound exhibit figure of merit (ZT) equal to unity for p-/n-type between -0.1 and $+0.05$ $\mu(\text{eV})$ at all temperatures, and $\text{Sr}_3\text{Ti}_2\text{O}_7$ compound exhibit ZT equal to unity for p-/n-type between -0.1 and $+0.02$ $\mu(\text{eV})$. $\text{Sr}_4\text{Ti}_3\text{O}_{10}$ exhibit ZT equal to unity for all temperatures in the p-type region, whereas in the n-type region it exhibits a unity at 300 K, 1.1 at 600 K and 1.2 at 900 K. While SrTiO_3 exhibit ZT equal to unity for p-/n-type between ∓ 0.1 $\mu(\text{eV})$ at all temperatures.

© 2014 Elsevier Ltd. All rights reserved.

1. Introduction

The $\text{Sr}_{n+1}\text{Ti}_n\text{O}_{3n+1}$ ($n=1, 2, 3, \infty$) Ruddlesden–Popper Homologous series are one of the promising oxide materials which attracted considerable interest. These materials are belong to the general formula $\text{A}_{n+1}\text{B}_n\text{O}_{3n+1}$, it composed of n perovskite blocks separated and sheared by rock-salt-structured layers along $(1/2)(111)$. They exhibit various unusual physical properties [1–6]. Owing to their wide energy band gap [1], $\text{Sr}_{n+1}\text{Ti}_n\text{O}_{3n+1}$ possess a wide range of electrical behavior varying from a high-dielectric-constant paraelectric in its undoped form to a superconductor when doped with a variety of elements [7]. $\text{Sr}_{n+1}\text{Ti}_n\text{O}_{3n+1}$ ($n=1, 2, 3, \infty$) compounds are good candidates as dielectric materials in capacitors, infrared detectors, oxygen ion conductors in sensors,

substrates for high T_c superconductors, or as piezoelectric materials in actuators [8–13]. A theoretical investigation for the atomic and the electronic structures of $\text{Sr}_{n+1}\text{Ti}_n\text{O}_{3n+1}$ ($n=1, 2, 3, \infty$) compounds was carried, it was found that the investigated compounds become unstable with respect to phase dissociation [14]. In 2003, Fennie and Rabe [15] perform density functional calculation for the structural and dielectric properties of $\text{Sr}_{n+1}\text{Ti}_n\text{O}_{3n+1}$ ($n=1$). An ab initio calculation was performed for the electronic structure and the optical conductivity of Sr_2MO_4 ($M=\text{Ti, V, Cr, Mn}$ and Co) [16].

To the best of our knowledge no comprehensive work neither experimental data nor theoretical calculations on the thermoelectric properties of $\text{Sr}_{n+1}\text{Ti}_n\text{O}_{3n+1}$ ($n=1, 2, 3, \infty$) Ruddlesden–Popper Homologous Series have appeared in the literature. Therefore as a natural extension to our previous work [17] a detailed depiction of the thermoelectric properties using full potential method is timely and would bring us important insights in understanding the transport properties of the investigated compounds. Hence it is very important to use a full potential method.

* New Technologies – Research Centre, University of West Bohemia, Univerzitni 8, 306 14 Pilsen, Czech republic. Tel.: +420 777 729 583.

E-mail address: maalidph@yahoo.co.uk.

2. Methodology

In $\text{Sr}_{n+1}\text{Ti}_n\text{O}_{3n+1}$ ($n = 1, 2, 3, \infty$) Ruddlesden–Popper Homologous series, the ($n = 1, 2, 3$) compounds are crystallizes in tetragonal structure ($I4/mmm$) whereas ($n = \infty$) compound belongs to the cubic structure ($\text{Pm}3m$) [18]. The crystal structure of the investigated compounds is represented in Fig. 1. For calculating the electronic band structures of $\text{Sr}_{n+1}\text{Ti}_n\text{O}_{3n+1}$ ($n = 1, 2, 3, \infty$) compounds we have employed the state-of-the-art full potential linear augmented plane wave plus local orbitals (FP-LAPW + lo) method as embodied in the WIEN2k code [19]. The exchange and correlation potential was described by the gradient approximation (GGA) [20], which is based on exchange-correlation energy optimization to calculate the total energy. In addition, we have used Engel–Vosko generalized gradient approximation (EV-GGA) [21] which optimizes the corresponding potential for electronic band structure calculations. The Kohn–Sham equations are solved using a basis of linear APW's. The potential and charge density in the muffin-tin (MT) spheres are expanded in spherical harmonics with $l_{\text{max}} = 8$ and nonspherical components up to $l_{\text{max}} = 6$. In the interstitial region the potential and the charge density are represented by Fourier series. Self-consistency is obtained using 500 k points in the irreducible Brillouin zone (IBZ). The convergence of the total energy in the self-consistent calculations is taken with respect to the total charge of the system with a tolerance 0.0001 electron charges.

To study the influence of vary “ n ” in $\text{Sr}_{n+1}\text{Ti}_n\text{O}_{3n+1}$ ($n = 1, 2, 3, \infty$) compounds on the thermoelectric properties, the semi-classical Boltzmann theory as implemented in the BoltzTraP code [22] was used. The thermoelectric transport tensors can be evaluated on the

base of calculated band structure using the standard Boltzmann kinetic transport theory and the rigid band approach [22]. The electrical conductivity $\sigma_{\alpha\beta}$, Seebeck coefficient $S_{\alpha\beta}$ and electronic thermal conductivity $k_{\alpha\beta}^0$ tensors are the main transport properties. We have calculated the thermoelectric properties using 5000 k points in the IBZ.

3. Results and discussion

3.1. Salient features of the electronic band structures

In order to get a reliable thermoelectric properties (transport properties), we required accurately calculated electronic band structure with reasonable k points in the IBZ and accurate exchange correlation potential. We have recalculated the electronic band structures of $\text{Sr}_{n+1}\text{Ti}_n\text{O}_{3n+1}$ ($n = 1, 2, 3, \infty$) compounds as represented in Fig. 2a–d. These figures suggested that the $\text{Sr}_{n+1}\text{Ti}_n\text{O}_{3n+1}$ ($n = 1, 2, 3, \infty$) compounds are indirect band gap semiconductors, with energy gap decreases with increasing the “ n ” from $1 \rightarrow \infty$. The calculated values of the energy gaps are 1.95, 1.89, 1.84, and 1.81 eV for $n = 1, 2, 3, \infty$, respectively. These values are less than the experimental values (3.25–3.5) eV [23,24]. For all cases the valence band maximum (VBM) is located at X point of the BZ, while the conduction band minimum (CBM) is situated at the center of the BZ. One can observe that moving from $n = 1 \rightarrow 2 \rightarrow 3$ the number of the band in the VBM and CBM are increases dramatically and shift the CBM towards the Fermi level. Whereas for $n \rightarrow \infty$ there is clear reduction in the number of the bands with reduce the value of the energy gap.

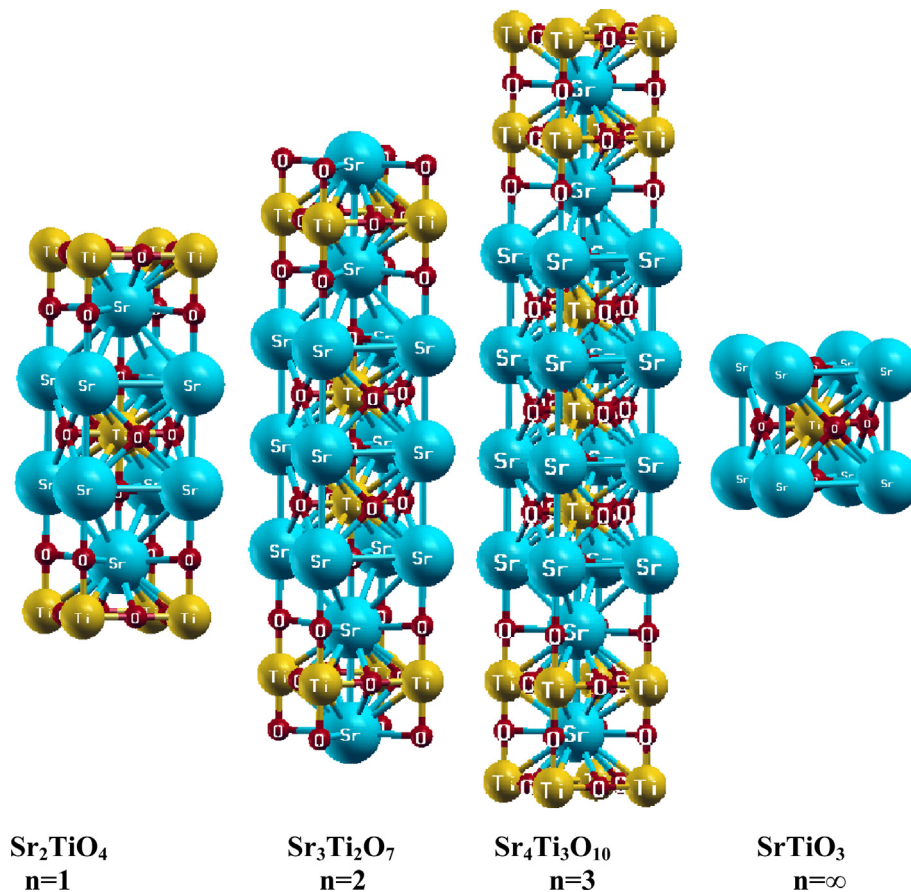


Fig. 1. Crystal structure of $\text{Sr}_{n+1}\text{Ti}_n\text{O}_{3n+1}$ ($n = 1, 2, 3, \infty$) Ruddlesden–Popper Homologous Series.

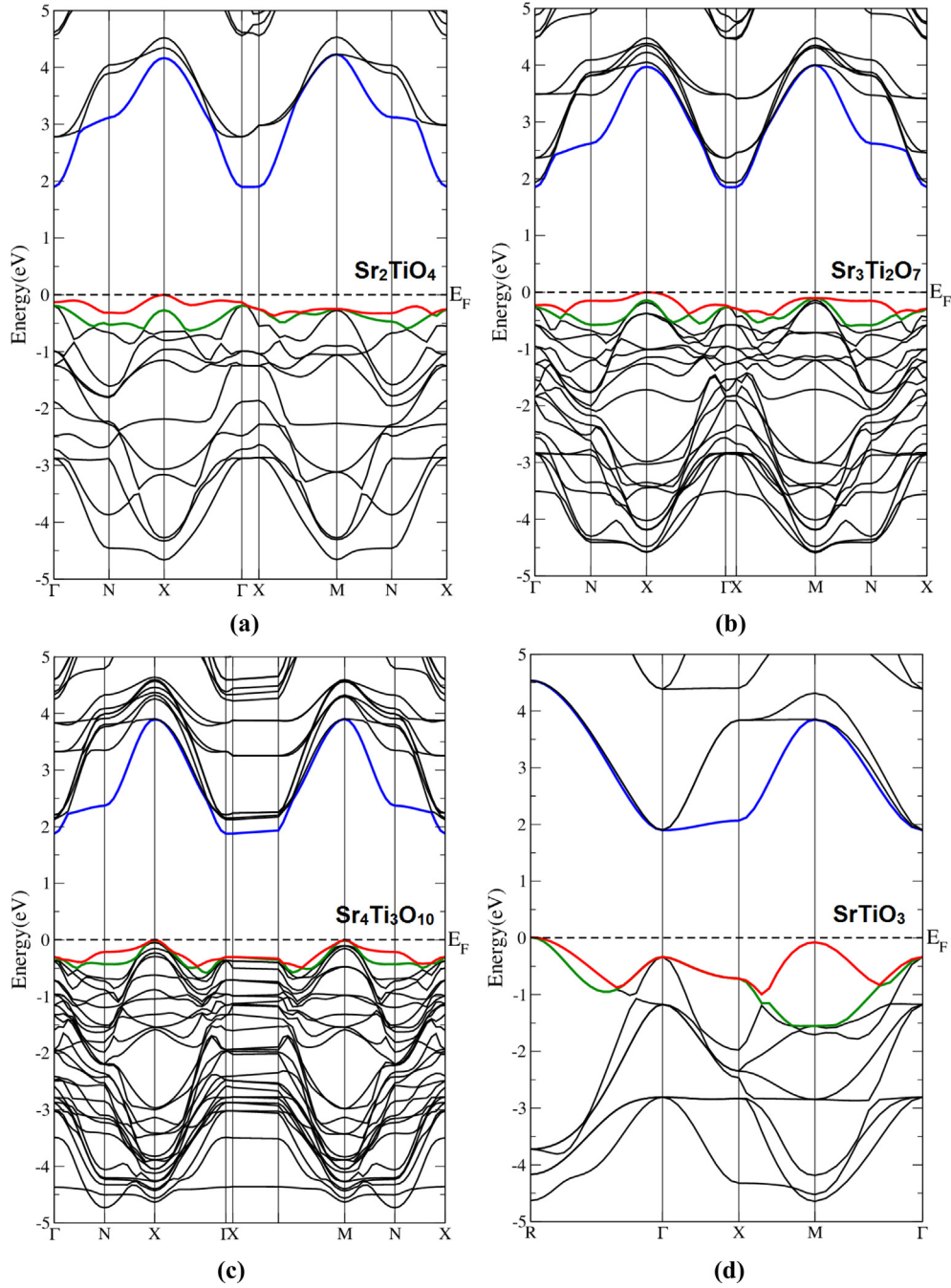


Fig. 2. The calculated electronic band structure of $\text{Sr}_{n+1}\text{Ti}_n\text{O}_{3n+1}$ ($n = 1, 2, 3, \infty$) Ruddlesden–Popper Homologous Series.

3.2. Effective mass

From the calculated electronic band structures, one can obtain the values of the effective masses and effective masses ratio. These values can be obtained from the curvature of the upper valence bands in the vicinity of X point of the BZ and the lower conduction bands around X point of the BZ. Usually we obtained these values through a simple parabolic fitting using the definition of effective mass as a second derivative of energy band with respect to the wave vector, k :

$$\frac{1}{m^*} = \frac{\partial^2 E(k)}{\hbar^2 \partial k^2} \quad (1)$$

Table 1

Calculated the electron effective mass ratio (m_e^*/m_e), effective mass of the heavy holes (m_{hh}^*/m_e) and light holes (m_{lh}^*/m_e), around Γ point the center of the BZ for $\text{Sr}_{n+1}\text{Ti}_n\text{O}_{3n+1}$ ($n = 1, 2, 3, \infty$) compounds.

Compound	m_e^*/m_e	m_{hh}^*/m_e	m_{lh}^*/m_e
Sr_2TiO_4	0.02701	0.03432	0.01807
$\text{Sr}_3\text{Ti}_2\text{O}_7$	0.02534	0.05615	0.11687
$\text{Sr}_4\text{Ti}_3\text{O}_{10}$	0.06888	0.02609	0.01789
SrTiO_3	0.02418	0.02357	0.01788

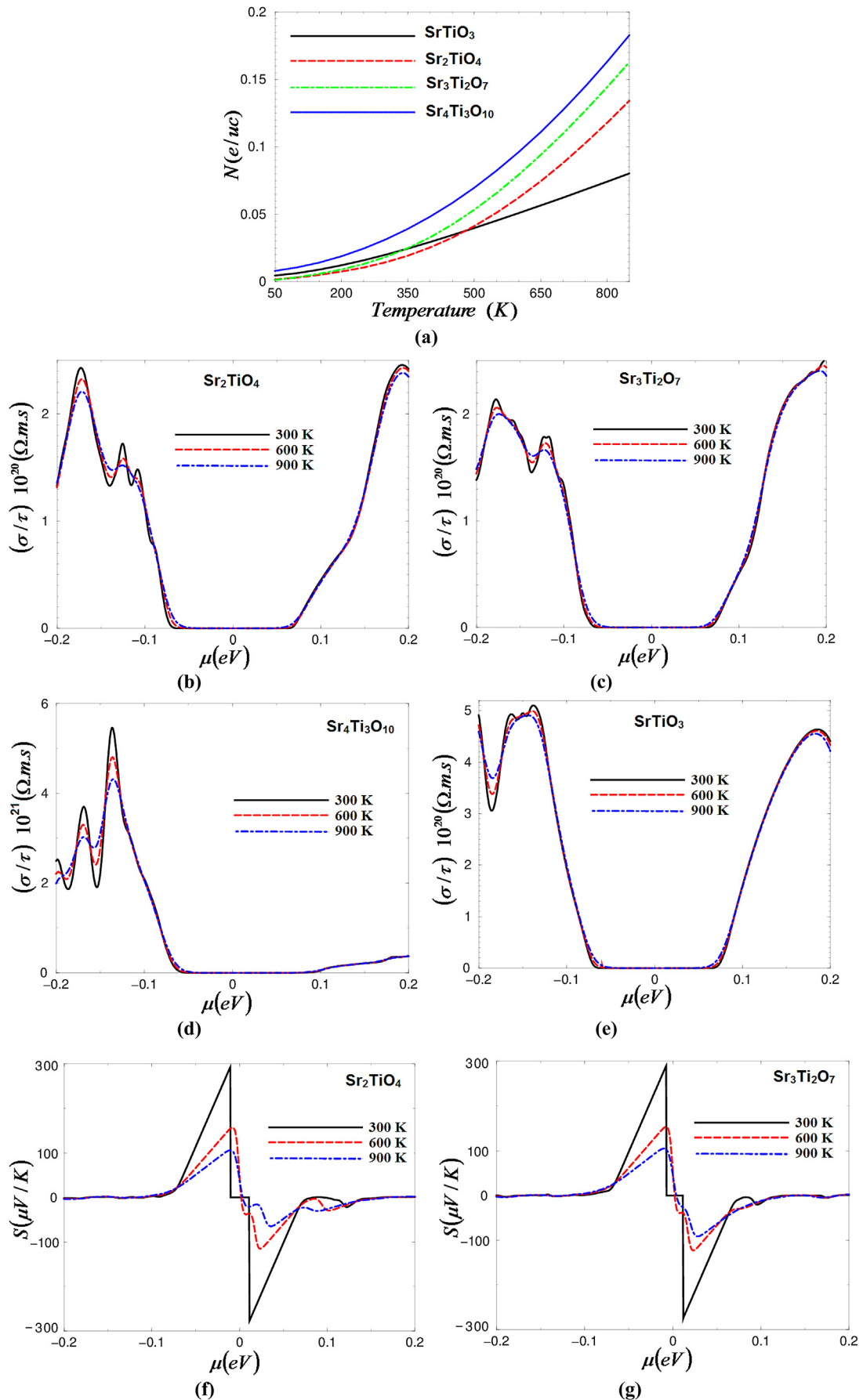


Fig. 3. The calculated transport properties as a function of chemical potential at three constant temperatures 300, 600 and 900 K of $\text{Sr}_{n+1}\text{Ti}_n\text{O}_{3n+1}$ ($n = 1, 2, 3, \infty$) Ruddlesden–Popper Homologous Series; (a) carriers concentration; (b–e) electrical conductivity; (f–i) Seebeck coefficient; (j–m) electronic thermal conductivity; (n–q) power factor; (r–u) figure of merit.

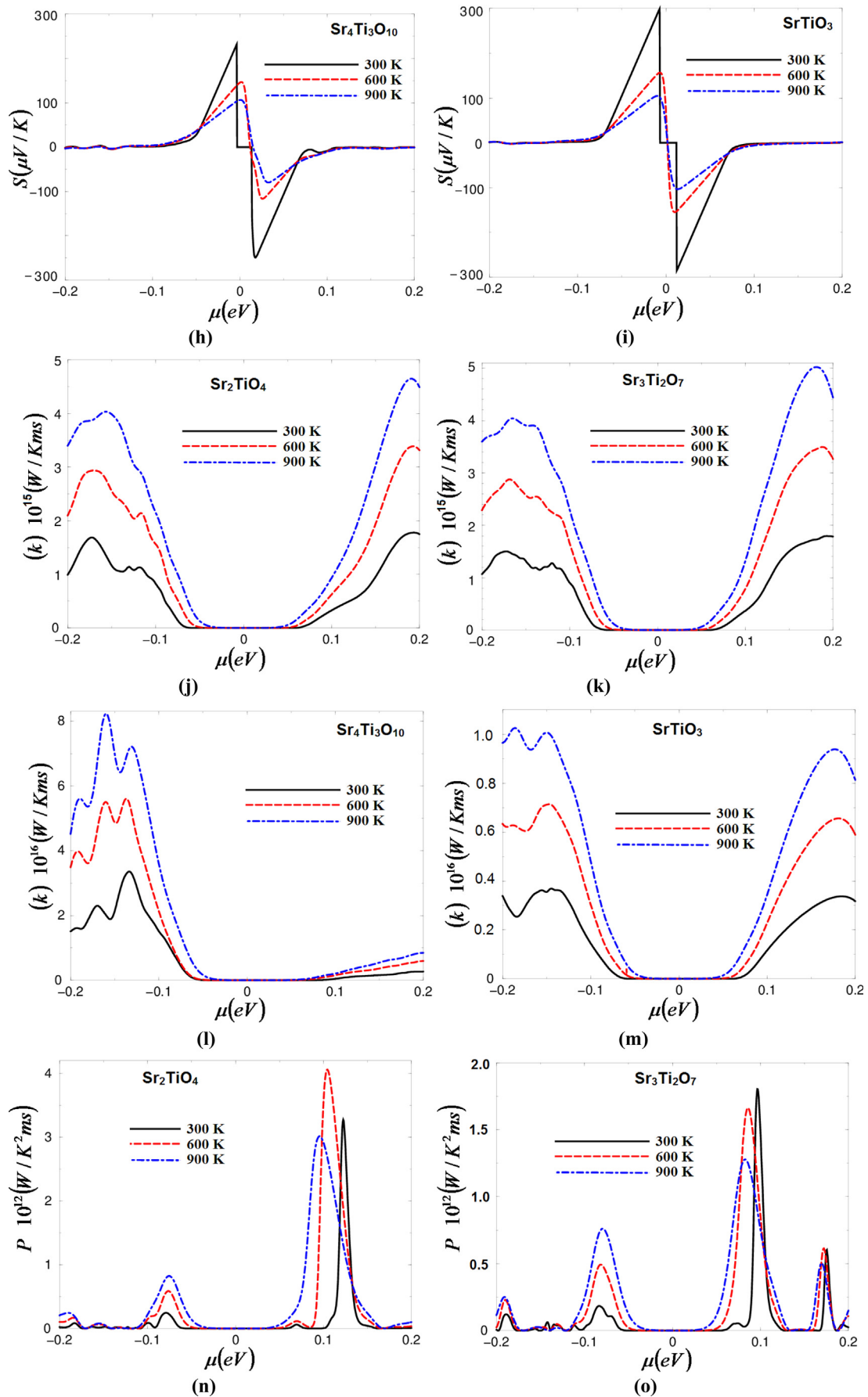


Fig. 3. (continued).

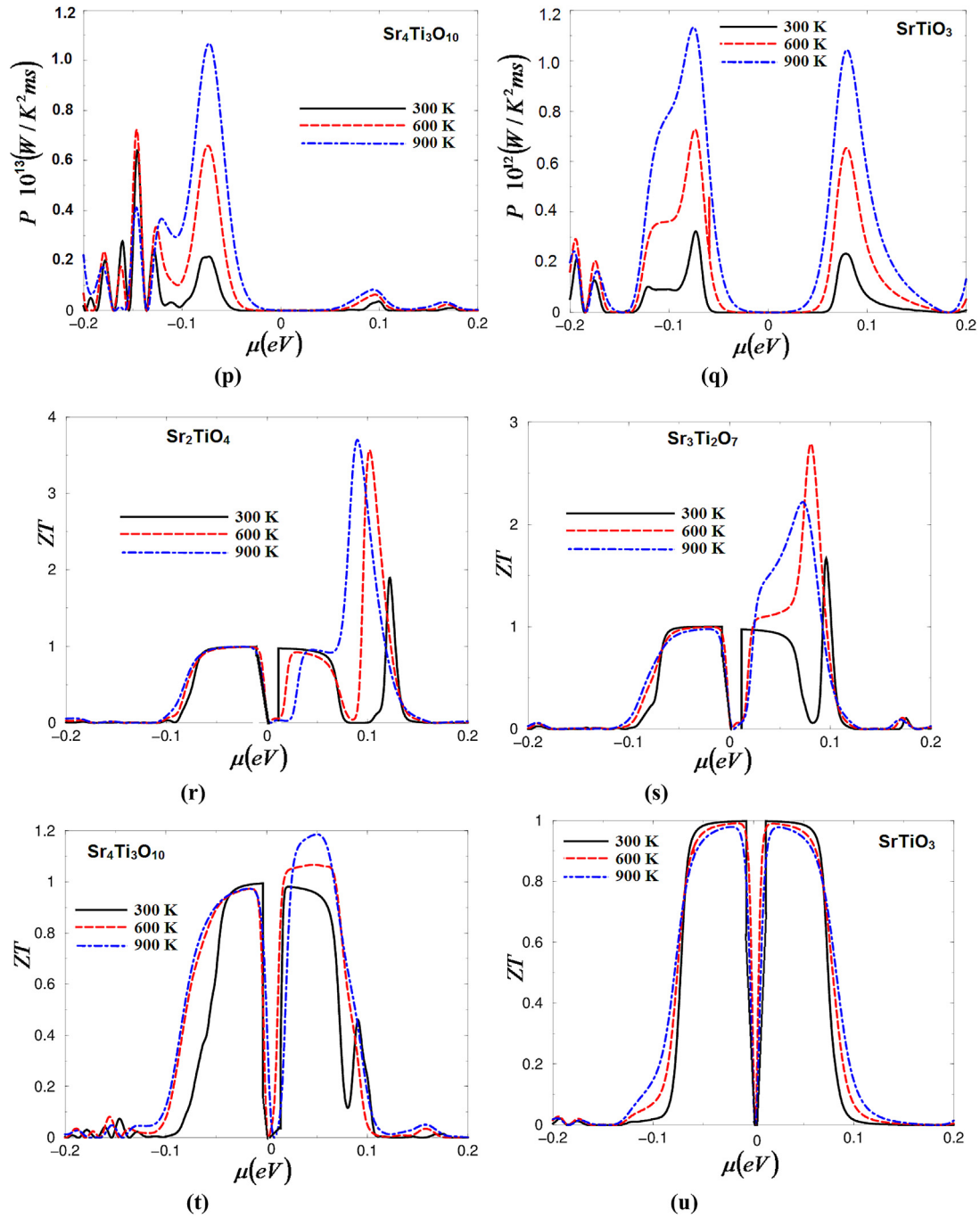


Fig. 3. (continued).

One can calculate the curvature of the VBM following the assumption that, if the spin–orbit interaction were neglected, the top of the valence band would have a parabolic behavior; this implies that the highest valence bands are parabolic in the vicinity of the point Γ . We should emphasize that the $\text{Sr}_{n+1}\text{Ti}_n\text{O}_{3n+1}$ ($n = 1, 2, 3, \infty$) compounds satisfy the parabolic condition of the VBM at Γ point. Based on the above assumption we have calculated electron effective mass ratio (m_e^*/m_e), heavy holes (m_{hh}^*/m_e) and light holes (m_{lh}^*/m_e) effective masses ratio. These values were listed in Table 1. It is clear that the larger the band curvature, the smaller the effective mass. The mean velocity of the electron is also found from $E(\vec{k})$, according to the relation

$$\vec{v}_{\vec{k}} = \frac{\partial E(\vec{k})}{\hbar \partial \vec{k}} \quad (2)$$

For this reason the energy dispersion relations $E(\vec{k})$ are very important in the determination of the transport properties for carriers in solids. From the electronic band structure diagram (Fig. 2) one would expect that hole carriers could be thermally excited to a second band at the X point. At room temperature, the X point hole carriers contribute significantly to the transport properties. Therefore, with accurately calculated band structure, and electron velocities we were able to calculate the transport properties.

Table 2
The values of the electric conductivity ($\Omega \text{ m s}^{-1}$) at $\pm 0.2 \mu(\text{eV})$ for $\text{Sr}_{n+1}\text{Ti}_n\text{O}_{3n+1}$ ($n = 1, 2, 3, \infty$) compounds.

Temp.	Sr_2TiO_4		$\text{Sr}_3\text{Ti}_2\text{O}_7$		$\text{Sr}_4\text{Ti}_3\text{O}_{10}$		SrTiO_3	
	p-type	n-type	p-type	n-type	p-type	n-type	p-type	n-type
300 K	-1.4×10^{20}	2.4×10^{20}	-1.4×10^{20}	2.5×10^{20}	-2.5×10^{21}	0.2×10^{21}	-4.9×10^{20}	4.4×10^{20}
600 K	-1.4×10^{20}	2.4×10^{20}	-1.5×10^{20}	2.5×10^{20}	-2.1×10^{21}	0.2×10^{21}	-4.7×10^{20}	4.4×10^{20}
900 K	-1.4×10^{20}	2.3×10^{20}	-1.5×10^{20}	2.3×10^{20}	-2.0×10^{21}	0.2×10^{21}	-4.6×10^{20}	4.3×10^{20}

3.3. Thermoelectric properties

The electrical conductivity can be written as $\sigma = ne\mu$, where n and μ are the carriers (electrons and holes) concentration and their mobility. The electrons and holes motilities can be written as $\mu_e = e\tau_e/m_e^*$ and $\mu_h = e\tau_h/m_h^*$. It is clear that the effective masses of electrons and holes have big influence on the motilities of the charge carriers, therefore the carriers with the smallest the effective mass the highest mobility. To increase the mobility one needs to rise the temperature, since the temperature increases the charge carrier's mobility increases, resulting in enhance the electrical conductivity to reach its maximum value. In general materials with high electrical conductivity are promising candidates for thermoelectric devices. In Fig. 3a we have represented the charge carrier's concentration of $\text{Sr}_{n+1}\text{Ti}_n\text{O}_{3n+1}$ ($n = 1, 2, 3, \infty$) compounds as a function of temperature. It is clear that moving from $n = 1 \rightarrow 2 \rightarrow 3$ led to increase the concentration of the charge carriers exponentially with increasing the temperature to reach its maximum values at 850 K. Whereas for the $n \rightarrow \infty$ case the charge carrier's concentration increases linearly with increasing the temperature to achieve the maximum value at 850 K. The maximum values of the charge carrier's concentration for $\text{Sr}_{n+1}\text{Ti}_n\text{O}_{3n+1}$ ($n = 1, 2, 3, \infty$) compounds are 0.3, 0.16, 0.18 and 0.08e/uc, respectively. These values suggested that $\text{Sr}_4\text{Ti}_3\text{O}_{10}$ compound exhibit the highest charge carrier's concentration along the temperature scale.

Fig. 3b–e represent the electrical conductivity of $\text{Sr}_{n+1}\text{Ti}_n\text{O}_{3n+1}$ ($n = 1, 2, 3, \infty$) compounds as a function of chemical potential at three constant temperatures (300, 600 and 900) K. We can observe that the $\text{Sr}_{n+1}\text{Ti}_n\text{O}_{3n+1}$ ($n = 1, 2, 3, \infty$) compounds exhibit the same critical points of the chemical potential for the electrical conductivity in p-type and n-type region at $\mp 0.2 \mu(\text{eV})$. The $\text{Sr}_{n+1}\text{Ti}_n\text{O}_{3n+1}$ ($n = 1, 2$) compounds achieved its highest electrical conductivity at $0.2 \mu(\text{eV})$ for n-type region (see Table 2). Whereas the $\text{Sr}_{n+1}\text{Ti}_n\text{O}_{3n+1}$ ($n = 3, \infty$) compounds achieved its highest value of electrical conductivity at $-0.2 \mu(\text{eV})$ for p-type region (see Table 2). It is clear that the $\text{Sr}_{n+1}\text{Ti}_n\text{O}_{3n+1}$ ($n = 1, 2, \infty$) compounds exhibit the same trends with vary the chemical potential and the temperature, whereas $\text{Sr}_4\text{Ti}_3\text{O}_{10}$ compound show different behavior that is attributed to the high number of O atoms which possess high electronegativity (3.44) in comparison to Ti (1.54) and Sr (0.95) atoms. Therefore, the charge density is substantially attracted toward O atoms due to their high electronegativity. One can see that at the chemical potential ranges between $\mp 0.05, \mp 0.06$ and $\mp 0.07 \mu(\text{eV})$, at 300, 600 and 900 K, respectively for the $\text{Sr}_{n+1}\text{Ti}_n\text{O}_{3n+1}$ ($n = 1, 2, \infty$) compounds and at $-0.04, -0.05, +0.07, +0.08 \mu(\text{eV})$ at 300, 600 and 900 K, respectively for the $\text{Sr}_4\text{Ti}_3\text{O}_{10}$ compound, these materials exhibit the minimum value of electrical conductivity, which is represent the regions where the investigated materials can give its maximum efficiency.

The Seebeck coefficient (S) can be written as a function of temperature and chemical potential [22] as follow;

$$S_{\alpha\beta}(T, \mu) = \frac{1}{eT\Omega\sigma_{\alpha\beta}(T, \mu)} \int \sigma_{\alpha\beta}(\varepsilon)(\varepsilon - \mu) \times \left[-\frac{\partial f_0(T, \varepsilon, \mu)}{\partial \varepsilon} \right] d\varepsilon \quad (3)$$

where Ω is the volume of the unit cell, and f_0 is Fermi-Dirac distribution function. Following the above equation, we have calculated Seebeck coefficient (S) of the $\text{Sr}_{n+1}\text{Ti}_n\text{O}_{3n+1}$ ($n = 1, 2, 3, \infty$) compounds as a function of chemical potential at 300, 600 and 900 K. These are represented in Fig. 3f–i. We would like to highlight that positive sign of S is related to p-type charge carriers, whereas the negative sign of S represent the n-type charge carrier. Following Fig. 3f–i, one can observe that S show one peak for p-type and one valley for n-type, at the vicinity of E_F . In all cases the highest value of Seebeck coefficient occurs at 300 K then it decreases with increasing the temperature. The values of $+S$ for p-type $\text{Sr}_{n+1}\text{Ti}_n\text{O}_{3n+1}$ ($n = 1, 2, \infty$) compounds are 300 ($\mu\text{V/K}$) while it is 250 ($\mu\text{V/K}$) for p-type $\text{Sr}_4\text{Ti}_3\text{O}_{10}$ compound. The $-S$ values for n-type $\text{Sr}_{n+1}\text{Ti}_n\text{O}_{3n+1}$ ($n = 1, 2, \infty$) compounds are 290 ($\mu\text{V/K}$), whereas it is 250 ($\mu\text{V/K}$) for n-type $\text{Sr}_4\text{Ti}_3\text{O}_{10}$ compound. One can observe that the $\text{Sr}_4\text{Ti}_3\text{O}_{10}$ compound show the lowest values of $\pm S$ at p-/n-type regions. It is important to mention that the critical points of $\pm S$ for p-type and n-type are $\mp 0.2 \mu(\text{eV})$ the range where $\text{Sr}_{n+1}\text{Ti}_n\text{O}_{3n+1}$ ($n = 1, 2, 3, \infty$) compounds exhibit very good thermoelectric properties, and beyond these points $\pm S$ is vanishes.

The thermal conductivity mathematically can be written as [22];

$$\kappa_{\alpha\beta}^0(T, \mu) = \frac{1}{e^2 T} \int \sigma_{\alpha\beta}(\varepsilon)(\varepsilon - \mu)^2 \left\{ -\frac{\partial f_0(T, \varepsilon, \mu)}{\partial \varepsilon} \right\} d\varepsilon \quad (4)$$

In general the thermal conductivity ($k = k_e + k_l$) consist of two parts, the electronic part k_e in which the electrons and holes transporting heat and the phonon part k_l represents the phonons traveling through the lattice. It is important to highlight the important fact that the BoltzTraP code calculates only the electronic part k_e . Materials with low thermal conductivity are considered to be the most promising candidates for designing the efficient thermoelectric devices. Therefore, we are interested to calculate the electronic thermoelectric conductivity of $\text{Sr}_{n+1}\text{Ti}_n\text{O}_{3n+1}$ ($n = 1, 2, 3, \infty$) compounds at three different temperatures as a function of chemical potential between $\mp 0.2 \mu(\text{eV})$ as shown in Fig. 3j–m. At the chemical potential ranges between $\mp 0.05, \mp 0.06$ and $\mp 0.07 \mu(\text{eV})$, at 300, 600 and 900 K, respectively for the $\text{Sr}_{n+1}\text{Ti}_n\text{O}_{3n+1}$ ($n = 1, 2, \infty$) compounds and at $-0.04, -0.05, +0.07, +0.08 \mu(\text{eV})$ at 300, 600 and 900 K, respectively for the $\text{Sr}_4\text{Ti}_3\text{O}_{10}$ compound, these materials exhibit the minimum value of electronic thermal conductivity, which is represent the regions where the investigated materials can give its maximum efficiency. The maximum values of the electronic thermal conductivity for p-type and n-type of the investigated materials at 300, 600 and 900 K are listed in Table 3, which show that $\text{Sr}_4\text{Ti}_3\text{O}_{10}$ compound exhibit the highest values of electronic thermal conductivity for p-/n-type regions at $\mp 0.2 \mu(\text{eV})$ for 300, 600 and 900 K.

The existence information on S and σ/τ helps to evaluate the power factor (P) since P is directly proportional to S^2 times σ/τ according to the formula $P = S^2(\sigma/\tau)$. We should emphasize that P is very important quantity for calculating the transport properties of the thermoelectric materials since it come as a numerator of the figure of merit relation ($ZT = PT/\kappa_e$). Therefore, we have

Table 3The maximum values of the electronic thermal conductivity in (W/K m s) at ± 0.2 μ (eV) for $\text{Sr}_{n+1}\text{Ti}_n\text{O}_{3n+1}$ ($n = 1, 2, 3, \infty$) compounds.

Temp.	Sr_2TiO_4		$\text{Sr}_3\text{Ti}_2\text{O}_7$		$\text{Sr}_4\text{Ti}_3\text{O}_{10}$		SrTiO_3	
	p-type	n-type	p-type	n-type	p-type	n-type	p-type	n-type
300 K	1.0×10^{15}	1.8×10^{15}	1.1×10^{15}	1.8×10^{15}	1.6×10^{16}	0.2×10^{16}	3.4×10^{15}	3.2×10^{15}
600 K	2.1×10^{15}	3.3×10^{15}	2.3×10^{15}	3.3×10^{15}	3.6×10^{16}	0.6×10^{16}	6.4×10^{15}	6.0×10^{15}
900 K	3.5×10^{15}	4.5×10^{15}	3.6×10^{15}	4.6×10^{15}	4.6×10^{16}	0.8×10^{16}	9.8×10^{15}	8.4×10^{15}

Table 4The peaks position of the power factor in μ (eV) for $\text{Sr}_{n+1}\text{Ti}_n\text{O}_{3n+1}$ ($n = 1, 2, 3, \infty$) compounds.

Temp.	Sr_2TiO_4		$\text{Sr}_3\text{Ti}_2\text{O}_7$		$\text{Sr}_4\text{Ti}_3\text{O}_{10}$		SrTiO_3	
	p-type	n-type	p-type	n-type	p-type	n-type	p-type	n-type
300 K	-0.07, -0.19	0.15	-0.07, -0.19	0.1, 0.17	-0.07, -0.13, -0.17, -0.18	0.1	-0.07, -0.17, -0.19	0.07
600 K	-0.07, -0.19	0.12	-0.07, -0.19	0.07, 0.17	-0.07, -0.13, -0.17, -0.18	0.1	-0.07, -0.17, -0.19	0.07
900 K	-0.07, -0.19	0.1	-0.07, -0.19	0.07, 0.17	-0.07, -0.13, -0.17, -0.18	0.1	-0.07, -0.17, -0.19	0.07

calculated P of the $\text{Sr}_{n+1}\text{Ti}_n\text{O}_{3n+1}$ ($n = 1, 2, 3, \infty$) compounds at 300, 600 and 900 K as a function of chemical potential between ∓ 0.2 μ (eV) as shown in Figs. 3n–q. Following these figure one can observe that the minimum values of P occurs at the vicinity of E_F . This could be due to the fact that σ/τ possesses minimum values in the vicinity of E_F . Beyond the chemical potential ranges ∓ 0.05 μ (eV) at 300 K, ∓ 0.06 μ (eV) at 600 K and ∓ 0.07 μ (eV) at 900 K for $\text{Sr}_{n+1}\text{Ti}_n\text{O}_{3n+1}$ ($n = 1, 2, \infty$) compounds and beyond -0.04 μ (eV) at 300 K, -0.05 μ (eV) at 600 and 900 K, $+0.07$ μ (eV) at 300 K, and $+0.08$ μ (eV) at 900 K for $\text{Sr}_4\text{Ti}_3\text{O}_{10}$ compound, these materials exhibit the maximum value of P , which represent the regions where the investigated materials can give its maximum efficiency. There exist pronounced peaks for p-/n-type of the investigated materials. The location of these peaks is listed in Table 4. It is clear that for all compounds the highest power factor occurs at 900 K, then it decreases with decreasing the temperature.

It is well known that the thermoelectric materials which have a figure of merit ($ZT = PT/\kappa_e$) about unity or greater than unity are considered to be promising candidates for thermoelectric devices [25,26]. Following the above formula, ZT is directly proportional to S^2 and σ/τ , and inversely proportional to κ_e . Thus, to increase ZT value one should reduce κ_e and increase $P = S^2\sigma$. Fig. 3r–u exhibits the calculated ZT for $\text{Sr}_{n+1}\text{Ti}_n\text{O}_{3n+1}$ ($n = 1, 2, 3, \infty$) compounds at 300, 600 and 900 K as a function of chemical potential between ∓ 0.2 μ (eV). It is clear that Sr_2TiO_4 compound exhibit a unity of ZT for p-/n-type between -0.1 and $+0.05$ μ (eV) at all temperatures. While $\text{Sr}_3\text{Ti}_2\text{O}_7$ compound exhibit ZT equal to unity for p-/n-type between -0.1 and $+0.02$ μ (eV). Then beyond $+0.05$ and $+0.02$ μ (eV) Sr_2TiO_4 and $\text{Sr}_3\text{Ti}_2\text{O}_7$ exhibit very sharp rise. Following Fig. 3r–u one can observe that $\text{Sr}_4\text{Ti}_3\text{O}_{10}$ exhibit ZT equal to unity for all temperatures in the p-type region, whereas in the n-type region it exhibit a unity at 300 K, 1.1 at 600 K and 1.2 at 900 K. While SrTiO_3 exhibit a unity ZT for p-/n-type between ∓ 0.1 μ (eV) at all temperatures.

To the best of our knowledge, there are no comprehensive work neither experimental data or first principles calculations on the thermoelectric properties of pure $\text{Sr}_{n+1}\text{Ti}_n\text{O}_{3n+1}$ ($n = 1, 2, 3, \infty$) Ruddlesden–Popper Homologous series are available in the literature to make a meaningful comparison. But we would like to mention here that in our previous work [27] we have calculated the thermoelectric properties of graphene using the same method of this work [19,22] and we found very good agreement with the experimental data. Thus, we believe that our calculations reported in this paper would produce very accurate and reliable results.

4. Conclusions

The electronic band structure calculation were performed using the state-of-the-art full potential linear augmented plane wave plus local orbitals (FP-LAPW + lo) method. Calculation exhibit that the valence band maximum located at X point of Brillouin zone (BZ), while the conduction band minimum is situated at the center of the BZ, resulting in an indirect band gaps of about 1.95, 1.89, 1.84, and 1.81 eV for $n = 1, 2, 3, \infty$, respectively. Based on the electronic band structure calculations, the transport properties of $\text{Sr}_{n+1}\text{Ti}_n\text{O}_{3n+1}$ ($n = 1, 2, 3, \infty$) Ruddlesden–Popper Homologous Series were evaluated using the semi-classical Boltzmann theory as implemented in the BoltzTraP code. The calculated charge carrier's concentration at 300, 600 and 900 K, show that $\text{Sr}_4\text{Ti}_3\text{O}_{10}$ compound exhibit the highest charge carrier's concentration along the temperature scale. We calculated the electrical conductivity and electronic thermal conductivity, and found that in the vicinity of Fermi level these materials exhibit the minimum value of electrical conductivity and electronic thermal conductivity, which represent the regions where the investigated materials can give its maximum efficiency. For all compounds the highest value of Seebeck coefficient occurs at 300 K then it decreases with increasing the temperature. These materials exhibit the maximum value of power factor (P) beyond the vicinity of Fermi level, which is represent the regions where the investigated materials can give its maximum efficiency. The investigated compounds exhibit figure of merit (ZT) about unity or greater than unity.

Acknowledgments

The work was supported by CENTEM Project, reg. no. CZ.1.05/2.1.00/03.0088, co-funded by the ERDF as part of the Ministry of Education, Youth and Sports OP RDI program. Computational resources were provided by MetaCentrum (LM2010005) and CERIT-SC (CZ.1.05/3.2.00/08.0144) infrastructures.

References

- [1] Blazey KW. Phys Rev Lett 1971;27:146.
- [2] Fujishita H, Shiozaki Y, Sawaguchi E. J Phys Soc Jpn 1979;46:581.
- [3] Marques MI, Arago C, Gonzalo JA. Phys Rev B 2005;72:092103.
- [4] Feng T. Phys Rev B 1982;25:627.
- [5] Koonce CS, Cohen ML, Schooley JF, Hosler WR, Pfeiffer ER. Phys Rev 1967;163:380.
- [6] Kan D, Kanda R, Kanemitsu Y, Shimakawa Y, Takano M, Terashima T, et al. Appl Phys Lett 2006;88:191916.
- [7] Haeni JH, Theis CD, Schlom DG, Tian W, Pan XQ, Chang H, et al. Appl Phys Lett 2001;78:3292.

- [8] Gupta TK. *J Am Ceram Soc* 1990;73:1817.
- [9] Ravi Kumar V, Rodrigues RP, Dravid VP. *J Phys D* 1996;29:1799.
- [10] Browning ND, Buban JP, Moltaji HO, Pennycook SJ, Duscher G, Johnson UD, et al. *Appl Phys Lett* 1999;74:2638.
- [11] Ernst F, Kienzle O, Ruhle M. *J Eur Ceram Soc* 1999;19:665.
- [12] Crandles DA, Nicholas B, Dreher C, Homes CC, McConnell AW, Clayman BP, et al. *Phys Rev B* 1999;59:12842.
- [13] Leonhardt M, Jamnik J, Maier J. *Electrochem. Solid-State Lett* 1999;2:333.
- [14] Noguera C. *Philos Mag Lett* 2000;80:173.
- [15] Fennie CJ, Rabe KM. *Phys Rev B* 2003;68:184111.
- [16] Weng H, Kawazoe Y, Wan X, Dong J. *Phys Rev B* 2006;74:205112.
- [17] Reshak AH, Auluck S, Kityk I. *Jpn J Appl Phys* 2008;47:5516–20.
- [18] Galasso FS. *Structure and properties of inorganic solids*. Oxford, U.K: Pergamon; 1970. p. 179.
- [19] Blaha P, Schwarz K, Madsen GKH, Kvasnicka D, Luitz J. WIEN2k, an augmented plane wave plus local orbitals program for calculating crystal properties. Austria: Vienna University of Technology; 2001.
- [20] Perdew JP, Burke S, Ernzerhof M. *Phys Rev Lett* 1996;77:3865.
- [21] Engel E, Vosko SH. *Phys Rev B* 1993;47:13164.
- [22] Madsen GKH, Singh DJ. *Comput. Phys Commun* 2006;175:67–71.
- [23] Inaguma Y, Nagasawa D, Katsumata T. *Jpn J Appl Phys* 2005;44:761.
- [24] Matsuno J, Okimoto Y, Kawasaki M, Tokura Y. *Phys Rev Lett* 2005;95:176404.
- [25] Rabin O, Yu-Ming L, Dresselhaus MS. *Appl Phys Lett* 2001;79:81–3.
- [26] Takeuchi T. *Mater Trans* 2009;50:2359–65.
- [27] Reshak AH, Khan SA, Auluck S. *J Mater Chem C* 2014;2:2346–52.